Current Applied Physics 32 (2021) 91–97

Contents lists available at ScienceDirect

Current Applied Physics

journal homepage: www.elsevier.com/locate/cap

Ion tracks in ultrathin polymer films: The role of the substrate

Raquel Thomaz [a,b,*], Nathan W. Lima [b], Diego Teixeira [a], Leandro I. Gutierres [a], Igor Alencar [a,b,c], Christina Trautmann [d,e], Pedro L. Grande [b], Ricardo M. Papaléo [a]

[a] Interdisciplinary Center of Nanoscience and Micro-Nanotechnology, School of Technology, Pontifical Catholic University of Rio Grande do Sul, PUCRS, Av. Ipiranga 6681, Porto Alegre, 90619-900, Rio Grande do Sul, Brazil
[b] Institute of Physics, Federal University of Rio Grande do Sul, UFRGS, Av. Bento Gonçalves 9500, Porto Alegre, 91501-970, Rio Grande do Sul, Brazil
[c] Department of Physics, Federal University of Santa Catarina, UFSC, R. Roberto Sampaio Gonzaga s/n, Florianópolis, 88040-900, Santa Catarina, Brazil
[d] GSI Helmholtzzentrum für Schwerionenforschung, Planckstr. 1, Darmstadt, 64291, Hesse, Germany
[e] Fachbereich Materialwissenschaften, Technische Universität Darmstadt, Alarich-Weiss-Str. 2, Darmstadt, 64287, Hesse, Germany

ARTICLE INFO

Keywords:
Ion tracks
Low dimensional materials
Polymer thin films
Radiation effects

ABSTRACT

Surface damage produced by single MeV-GeV heavy ions impacting ultrathin polymer films has been shown to be weaker than those observed under bulk (thick film) conditions. The decrease in damage efficiency has been attributed to the suppression of long-range effects arising from excited atoms lying deeply in the solid. This raises the possibility that the substrate of the films itself is relevant to the radiation effects seen at the top surface. Here, the role of the substrate on cratering induced by individual 1.1 GeV Au ions in ultrathin poly(methyl methacrylate) (PMMA) layers is investigated. Materials of different thermal and electrical properties (Si, SiO_2, and Au) are used as substrates to deposit PMMA thin films of various thicknesses from ~1 to ~300 nm. We show that in films thinner than ~40 nm craters are modulated by the underlying substrate to a degree that depends on the transport properties of the medium. Crater size in ultrathin films deposited on the insulating SiO_2 is larger than in similar films deposited on the conducting Au layer. This is consistent with an inefficient coupling of the electronic excitation energy to the atomic cores in metals. On the other hand, the damage on films deposited on SiO_2 is not very different from the Si substrate with a native oxide layer, suggesting, in addition, poor energy transmission across the film/substrate interface. The experimental observations are also compared to calculations from an analytical model based on energy addition and transport from the excited ion track, which describe only partially the results.

1. Introduction

Swift heavy ions penetrating in a solid produce along their trajectory a narrow zone of a few nanometers in diameter where a huge amount of energy is deposited in the form of electronic excitation [1,2]. Part of this energy is rapidly transferred to the lattice, generating heat and stress pulses that further distribute the deposited energy and creates damage [3–5]. The extent of the damage is controlled by the efficiency of energy conversion from the electronic subsystem to the atomic cores, and is particularly large in insulators [6,7], where structural changes and various levels of chemical modifications are observed. The impinging ions may also induce sputtering and particle transport at the surface, leading to the formation of nanometer-sized structures, such as craters and extended protrusions. The shape and size of the craters depend on several factors related both to the properties of the materials (cohesive energy, crystal structure, molar mass, electrical conductivity, roughness) [8–11] and to the beam parameters, such as ion velocity, stopping power, charge state, and angle of incidence [12–15] (see also Refs [16, 17] for reviews). The fact that matter can be strongly transformed in very spatially confined regions by individual swift heavy ions has been the basis of a plethora of successful and relevant applications, from the engineering of nanostructured materials [18–20] to cancer treatment [21].

Ion irradiation of polymeric materials induces irreversible changes in their macromolecular structure, causing profound alterations in chemical and physical properties. Because of that, ion bombardment has been used as a tool for controlled tuning of both chemical composition and related physical properties of polymers [22,23]. One of the most

* Corresponding author. Interdisciplinary Center of Nanoscience and Micro-Nanotechnology, School of Technology, Pontifical Catholic University of Rio Grande do Sul, PUCRS, Av. Ipiranga 6681, Porto Alegre, 90619-900, Rio Grande do Sul, Brazil.
E-mail address: raquel.thomaz@pucrs.br (R. Thomaz).

https://doi.org/10.1016/j.cap.2021.10.004
Received 14 May 2021; Received in revised form 11 September 2021; Accepted 12 October 2021
Available online 20 October 2021

important commercial polymeric material is poly(methyl methacrylate) (PMMA). PMMA is a radiation sensitive polymer undergoing preferentially main chain-scission and cleavage of pendent methyl ester groups upon exposure to ion irradiation at room temperature [24–27]. Because of that, thin films based on PMMA have been widely used in microlithography with UV photons, x-rays, or electron beams [28–31], or in direct microstructuring processes such as proton beam writing [32,33]. More recently, PMMA has been used as the base-material for phantoms and beam-monitoring devices [34] in the growing field of proton radiotherapy [35,36]. Therefore, a deep understanding of the radiation effects in PMMA is important not only to evaluate the stability and behavior of this material under various high-energy radiation fields, but also to optimize procedures in modern ion beam-based processing techniques, where polymers play an important role [30–33,37].

Recent research has demonstrated, on the other hand, that when the size of irradiated objects is sufficiently small the strength of radiation to modify matter may differ from the bulk [38–42]. This behavior may originate from the increased role of surfaces and interfaces in controlling energy transport, or from the changes in the effective deposited energy per se [43,44]. Nevertheless, size-effects in irradiated nanostructured matter are still not well understood. In particular, we have recently shown that under the spatially confined conditions of ultrathin polymer films, the damage efficiency of swift heavy-ions is weakened. While the effect is moderate in bond-breaking processes [45], it is pronounced in surface effects related to large-scale particle motion such as cratering [46]. For cratering, the critical length below which confinement effects appear is relatively large [e.g., ~35–40 nm in PMMA], much larger than physical size restrictions that occur when the thickness of the film is comparable to the dimensions of crater features (of the order of 10 nm). The decrease in damage efficiency in thin polymer layers has been attributed to the suppression of long-range cooperative effects of excited atoms lying deep in the solid (which are otherwise present in thick layers) [46].

An important issue that arises from these findings regards the influence of the underlying substrate on the magnitude of the damage in ultrathin films. In a previous work using Si substrates [46], it was implicitly assumed that excitation in the Si has no contribution for cratering in PMMA films. This was based on the fact that electronic excitation in crystalline Si is quickly quenched, before significant conversion into atomic motion [47]. While this may be a reasonable ad-hoc assumption for Si, the contribution of the substrate cannot be a priori neglected, as we demonstrate in this work. Here, we provide direct experimental evidence that substrates of silicon dioxide, silicon, and gold have a different effect on damage produced in the films, if the film is sufficiently thin. This behavior is partially described by a simple analytical model based on energy addition and transport from the excited atoms along the ion track.

2. Materials and methods

Thin films of PMMA (Polymer Standards, molecular weight of ~130 ku) were deposited by means of spin coating on three different substrates: silicon dioxide (200 nm-thick film thermally grown on ~0.5 mm-thick Si wafers), silicon (with a ~2.3 nm native oxide layer), and gold (40 nm-thick film grown on Si wafers pre-coated with 5 nm of Ti). PMMA films of thicknesses h from ~1 nm up to 300 nm were prepared from anisole solutions and baked on a hot plate at 60 °C in order to allow relaxation of the film and removal of residual solvent. Table S1 presents a series of selected properties of the substrate and polymer materials, which are useful for the subsequent discussion of the data (see Supplementary Material for details).

The thicknesses of the films were measured by two different techniques: atomic force microscopy (AFM) and resonant Rutherford backscattering spectrometry (RRBS) through the reaction $^{12}C(\alpha, \alpha')^{12}C$ at 4.285 MeV [48]. RRBS was carried out using a 4.285 MeV He^+ beam delivered from a 3 MV Tandetron (High Voltage Engineering). The primary beam impinged at normal incidence to the surface of the samples and the scattered ions were collected at an angle of 165° with a surface-barrier, silicon charged-particle detector (17 keV resolution). Channel-to-energy conversion was performed using the high-energy edge signal from ions backscattered at a gold standard specimen. Data were analyzed using the SIMNRA software [49] with the appropriate non-Rutherford cross sections. The parameter *thickness* in units of atoms per cm^2 was varied in the SIMNRA calculations until a reasonable agreement with the experimental data was obtained, as shown in Fig. 1a and b. For the thickness conversion from atoms per cm^2 to nm, the value of the bulk density was employed (Table S1).

In the case of AFM, the thickness was obtained from the depth of trenches made on the films with a sharp scalpel as illustrated in Fig. 1c. All AFM measurements were performed in a Bruker Dimension Icon PT instrument in the Peak Force mode in air.

The irradiation with 1.1 GeV Au ions was performed at the UNILAC accelerator at GSI (Darmstadt, Germany) applying an ion fluence of 10^9 ions/cm^2 at normal incidence. The electronic stopping power of the ions in each material involved is given in Table S1 (see Supplementary Material).

The size and shape of the individual ion impact features were characterized offline by means of AFM also using the Peak Force mode in air. The images for surface track analysis were collected at a scan frequency of 1–2 Hz with 256 scan lines in 500 nm scans. The tips used were Bruker ScanAsyst-air (Silicon Nitride) with a nominal radius of 2 nm. In order to minimize tip-convolution effects, only images collected with high and similar quality tips were stored for quantitative analysis.

3. Results and discussion

3.1. Film thickness and roughness

Fig. 1 shows typical results of PMMA film thickness determination by RRBS and AFM. For the former, the area of the C peak was used, considering the appropriate cross section of the $^{12}C(\alpha, \alpha')^{12}C$ reaction. In Fig. 1, calculations by SIMNRA are represented by solid red lines, while experimental data by full black circles. The spectra shown in (a) and (b) correspond to films with thicknesses of 12 and 122 nm, respectively. In the AFM method, the depth of the trench created by a sharp scalpel directly gives the film thickness (Fig. 1c). In general, both techniques gave similar thickness values, but each possesses inherent limitations. The AFM scratch method is not adequate for films deposited on the relatively soft Au substrate and RBS relies on the knowledge of the film density, which may be slightly different from tabulated bulk values [50]. In the plots presented in this work, the thicknesses derived by the AFM profiles were used for films deposited on silicon and silicon dioxide, and by RRBS for films deposited on gold.

The as-deposited PMMA films prepared on Si and SiO_2 had a root mean square roughness R_q of about 0.25 nm (deduced from $1 \times 1\ \mu m^2$ AFM scans) for all thicknesses investigated. The roughness of the films deposited on Au was at similar levels only for layers thicker than about 12 nm (Fig. 1d). For thinner films, R_q was thickness-dependent, increasing progressively toward values close to the bare Au layer ($R_q = 0.68$ nm) as the film thickness was reduced (Fig. 1e and f). Adhesion of PMMA to Si and SiO_2 substrates is expected to be stronger than to Au due to the polar interactions between the oxide layer of the substrate and the side-chain ester groups of PMMA.

We also checked the chemical structure of the PMMA films by x-ray photoelectron spectroscopy and found no significant differences among films of different thicknesses or deposited on the distinct substrates.

3.2. Impact features

Fig. 2 presents AFM images of PMMA thin films of different thicknesses deposited on SiO_2, Si, and Au substrates bombarded by Au ions. For thick films ($h > 40$ nm), the impact structures are similar among

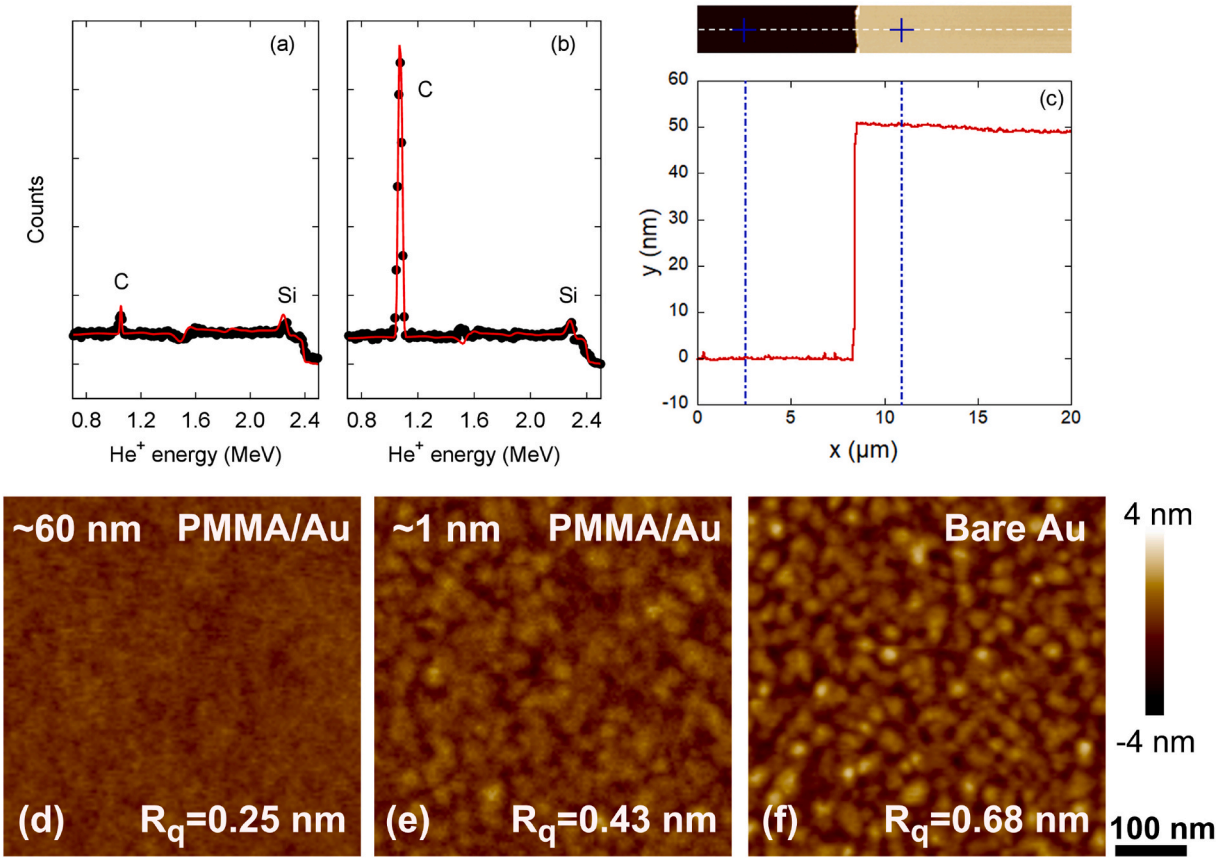

Fig. 1. Typical results for PMMA film thickness determination by AFM and RRBS. (a–b) Resonant RBS spectra of two PMMA films with thickness of (a) 12 nm and (b) 122 nm. Calculations performed with SIMNRA software [49] are represented by solid red lines, while experimental data by full black circles. Carbon and silicon signals are labeled in the spectra. (c) AFM image showing a region around a micro-scratch created on a 50 nm-thick film and the corresponding height section. (d–e) AFM images of ~60 nm-thick and ~1 nm-thick PMMA films deposited on Au. (f) AFM of a bare Au substrate. The RMS roughness is also given in each image. The image (d) represents the typical roughness of films on Si or SiO_2 substrates, independent of the thickness. (For interpretation of the references to colour in this figure legend, the reader is referred to the Web version of this article.)

different substrates, as expected. Each impact consists of a nanometer-sized crater surrounded by a rim of protruded material. These features typically appear on the surface of polymers and other organic materials bombarded by swift-heavy ions [16]. In films thinner than 40 nm, the rim size progressively decreases until they are completely suppressed. Craters also diminish with decreasing thickness but at a much slower pace than the rims and they are clearly visible even in the thinnest films analyzed. This general behavior is similar for the three investigated substrates and corroborates previous findings on the weakening of surface damage when the films are thinner than a given critical value h_c [46]. That is, h_c is a critical thickness below which crater and rim sizes become thickness-dependent. h_c can be extracted from the point of intersection of a horizontal line that projects the saturation (bulk) value of a given crater dimension with a straight line that follows the decay of the crater size at small thicknesses. For example, following this procedure, h_c for the crater diameter (Fig. 3b) is around 10 nm, but is larger for the rim volume (close to 30 nm, depending on the type of substrate, Fig. 3a). It is interesting to note that although the different dimensions displayed in Fig. 3 are related to each other, the critical thicknesses h_c for craters and rims are not unique. This has been described previously [46]: effects that strongly depend on the cooperative action of energy sources along the track (as rim formation) are suppressed first, resulting in large critical lengths. The crater hole diameter on the other hand is mainly defined by intense and localized excitation events that occurs close to the near surface, with little contribution from excitation from deep layers in the film.

There are, however, important differences in the thickness dependence of the impact features among the different substrates. Quantitative analysis of crater size displayed in Fig. 3 allows a more detailed view of such specificities. The surface feature most sensitive to the underlying substrate is the rim volume (Fig. 3a). The critical thickness h_c, below which the rim volume starts to decrease, clearly varies among the different substrates, specially between the insulating silicon dioxide and the conducting Au backing. For a film of ~20 nm deposited on Au, the rim volume has already decreased by ~70%, while for an equivalent film deposited on SiO_2, the rims still sustain volumes similar to the values found for thick films. Regarding craters, their diameter (D_{crater}, Fig. 3b) only slightly differs for the three substrates, whereas the crater depth (Z_{crater}, Fig. 3c) is susceptible to the nature of the underlying substrate. As an example, the crater depth in the 20 nm-thick PMMA film deposited on Au is ~3 times smaller than in the film on silicon dioxide or Si substrates.

The above observations indicate that the substrate is capable of directly influencing the energy available for the formation of craters on the polymer film. In order to analyze the substrate contribution from a theoretical standpoint, we applied the sum of impulses model [4], originally developed to describe sputtering of organic molecules, and recently used to describe size effects of cratering in ultrathin films [46]. The energized track is treated as a line of elemental point sources of excitation, each contributing with an energy ΔE_i that spreads diffusively in a dissipative medium [4]. The sum of all excitations generated at various depths z along the ion track results in the total deposited energy density $\varepsilon(\rho, z, t, h)$ at time t and radial distance ρ from the impact center, and the net impulse $\Delta\vec{p}$. This impulse is assumed to drive particle motion

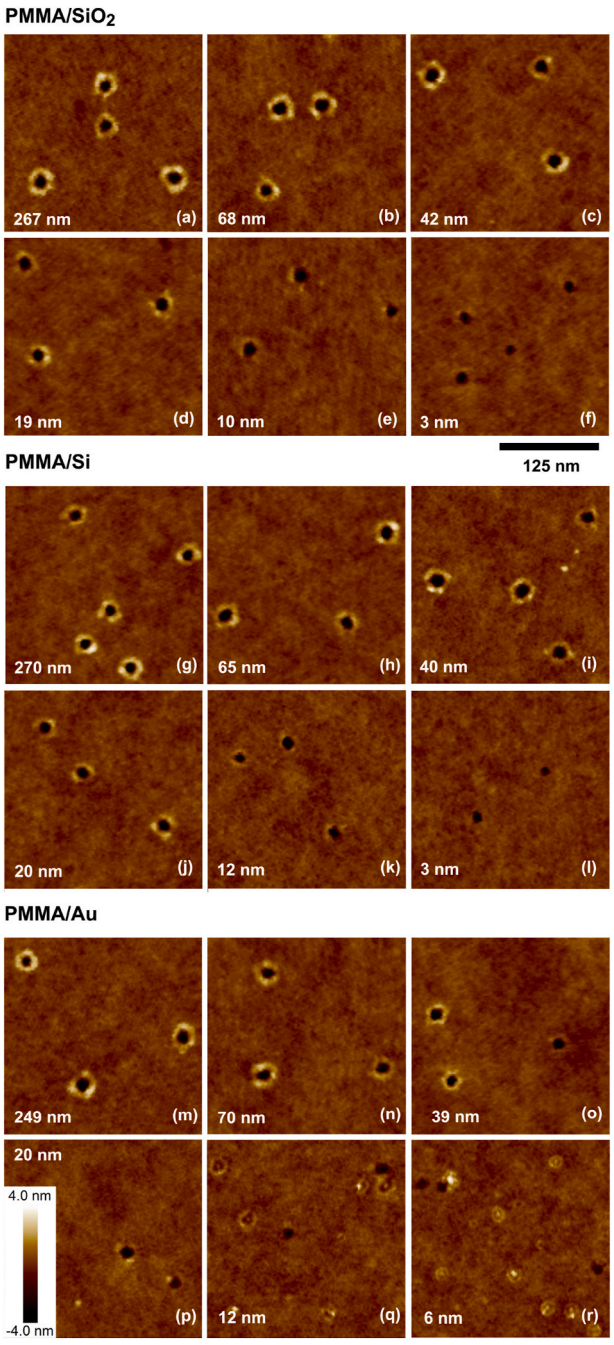

Fig. 2. AFM images of PMMA thin films of different thicknesses deposited on silicon dioxide (a–f), silicon (g–l), and Au (m–r) bombarded by 1.1 GeV Au ions at normal incidence. The thickness of the films is given in each image. For very thin films on Au substrate intrinsic defects appear, which are distinctively different from those produced by the ion impacts (q–r). (For interpretation of the references to colour in this figure legend, the reader is referred to the Web version of this article.)

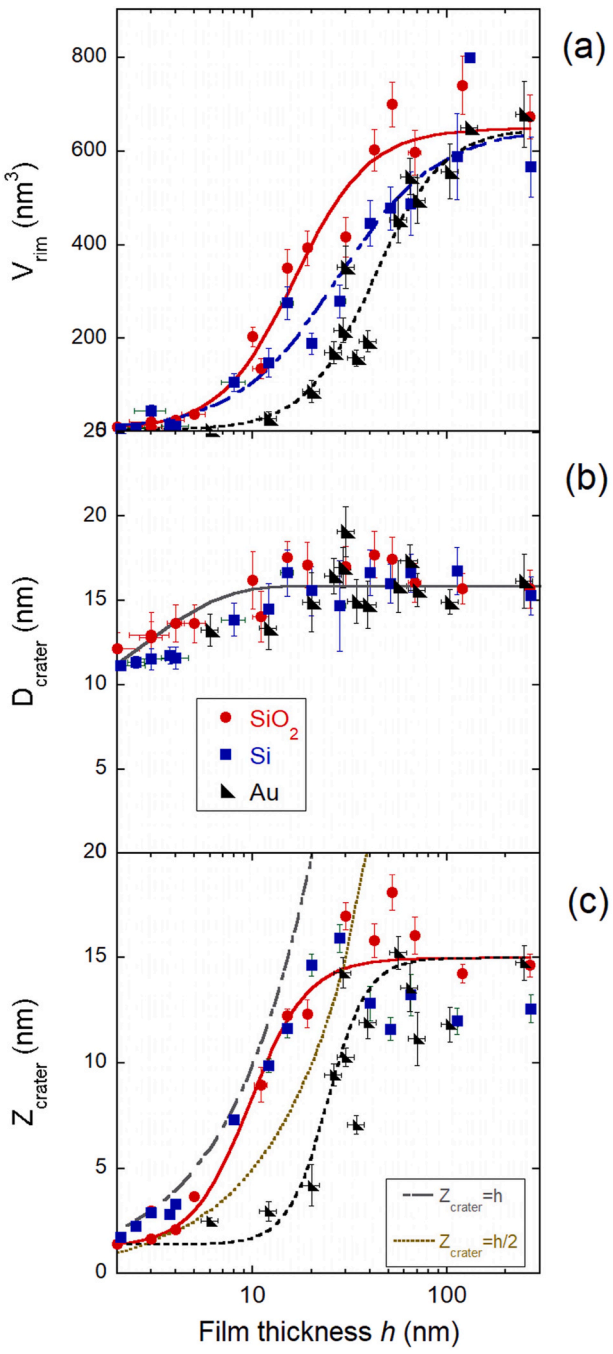

Fig. 3. Averaged rim and crater dimensions produced by 1.1 GeV Au ions in PMMA films of various thicknesses h deposited on Si, SiO_2 and Au substrates: (a) rim volume, (b) crater diameter, and (c) crater depth. The lines are guides to the eyes.

and ejection, leading to the formation of a crater. Particle ejection occurs if the net momentum transferred along the z direction p_z exceeds a critical value p_c. Thus, crater dimensions can be directly extracted from the volume of points in space with $p_z > p_c$. The crater rim volume can also be roughly estimated from the volume of material with $p_c^R < p_z < p_c$, where p_c^R is an impulse large enough for plastic deformation, but insufficient for ejection.

Impulses originating from the ion track segment lying in the substrate were ignored in our previous work [46] and are here included as an additional source of energy and momentum to the PMMA film. Using cylindrical coordinates, we solved numerically the 3-D equation for energy density diffusion from Ref. [4], taking into account the vacuum/film and film/substrate interfaces by using the boundary condition of flux conservation. From that, the final impulse maps are obtained (see Supplementary Material for further details). The input parameters for each material are the diffusivity δ, the rate of energy dissipation $1/\tau$, and the effective stopping power dE/dx_{eff}, which is associated to the fraction f of electronic energy converted into atomic motion ($dE/dx_{\text{eff}} = f \times dE/dx$). For PMMA, Si and SiO_2, it was considered that ~35% of the dE/dx is converted into atomic motion, as in Ref. [51]. For Au, it is well known that this coupling is very inefficient [52], therefore we assumed f

= 0.02. This value is supported by a comparison of lattice peak temperatures induced by 1 GeV Au in PMMA and Au, obtained from calculations with the inelastic thermal spike model [53]. As the thermal transport parameters under the short time conditions during track formation are not known, we used as a guide for the diffusivity tabulated bulk equilibrium room-temperature values (data presented in the Supplemenatry Material). For SiO_2, the thermal diffusivities found for thin layers were also used. The relaxation times τ were chosen to keep the relevant impulse integration time ($\sim 3\tau$) close to typical values of crater formation derived from molecular dynamic simulations using either Lennard-Jones or FENE potentials (around 50–100 ps [10,60]). We kept for PMMA a τ of 30 ps and the same $p_c = \sqrt{3mkT_c}$ used in a previous work, where the substrate was ignored (m is the monomer mass, k the Boltzmann constant, and T_c the ceiling temperature of PMMA). Relaxation times are expected to be increasingly larger in SiO_2, Si and Au, and were accordingly scaled based on THz phonon attenuation data [56].

The results of calculated crater dimensions in films deposited on substrates of Au and SiO_2 are given in Fig. 4a–c. These data were derived from maps in the $\rho - z$ plane of the normal component of the momentum (p_z). Some of them are presented in Fig. 4d–i. An extended set of maps, further exploring the effect of changing the input parameters on the calculations, is given in the Supplementary Material.

Under the conditions of the calculations described above, Au behaves as an inert substrate that does not contribute to cratering in the polymer film surface. PMMA on an Au substrate behaves very similar as the freestanding configuration (see maps in Fig. 4e and f) because of the low transfer efficiency of the electronic excitation to the lattice associated to the high electronic conductivity of gold. If an unrealistic larger value of f = 0.35 is applied, impulses from the Au substrate substantially enhance crater dimensions for ultrathin films (as e.g. in Fig. 4g). Whilst this is not observed experimentally for the high energy ions used in our experiment, the latter condition may be reached for ions in the nuclear stopping regime where momentum is directly transferred from the projectiles to the lattice atoms.

For the insulating SiO_2 substrate, the model predicts a strong influence on crater size and shape in ultrathin films. The crater diameter increases steadily for $h < 20$ nm (Fig. 4b). The crater depth also becomes larger than the value for thick films. But for films thinner than about 20 nm it starts to decrease, approaching the curve $Z_{crater} = h$, which is the maximum crater depth allowed by the physical size of the layer (Fig. 4c). Note that in the case of the Au backing, or in the freestanding configuration, the predicted maximum crater depth in the ultrathin films is smaller and limited to $Z_{crater} = h/2$ (see dashed lines in Fig. 4c). This arises from the symmetry of the impulse summation: the net momentum points upwards for points at $z < h/2$ and downwards when $z > h/2$ (Fig. 4e) [46]. The rim volumes also present a considerable

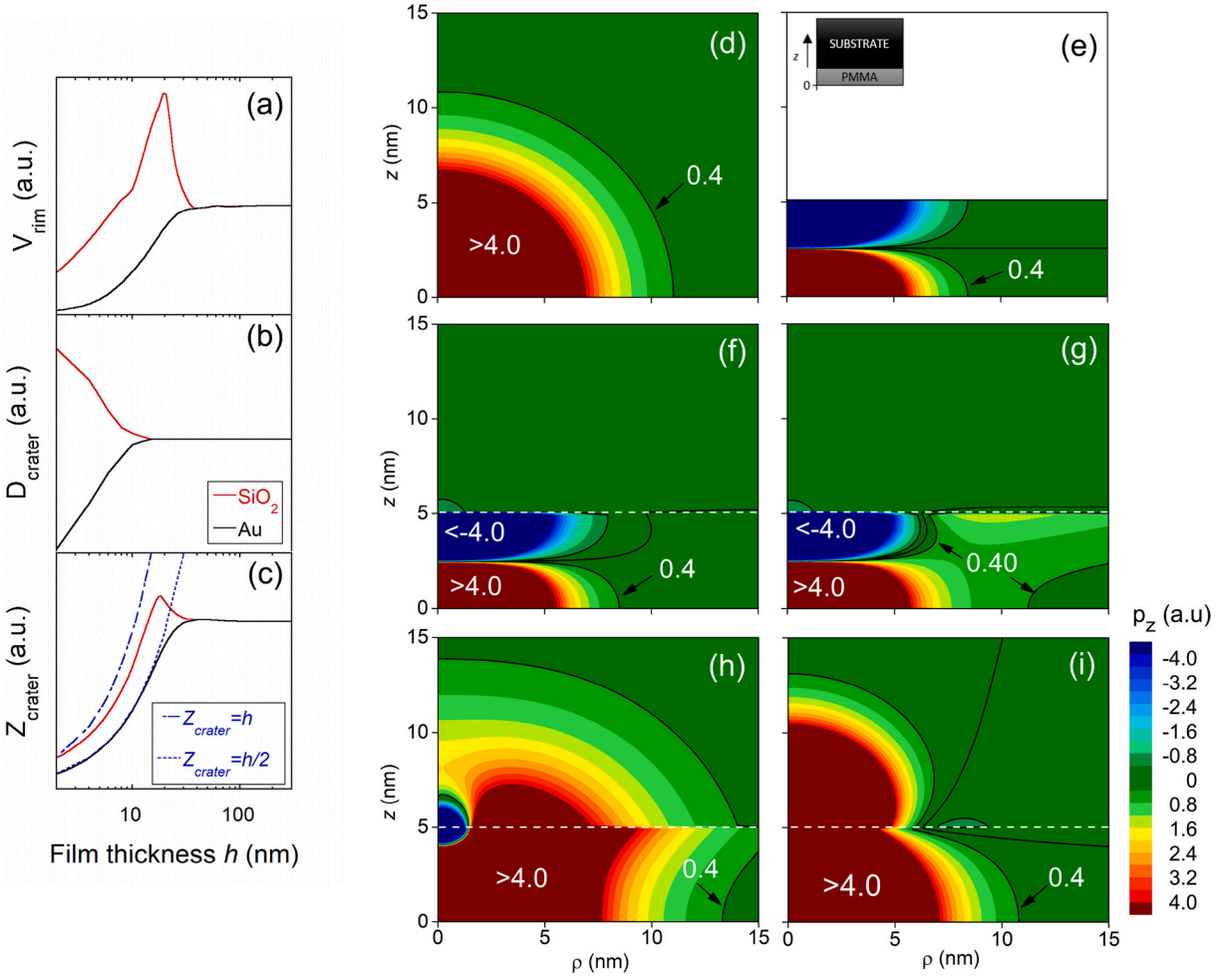

Fig. 4. Results of calculations from the sum of impulses model for films bombarded by 1.1 GeV Au ions at normal incidence. (a–c) Crater dimensions in PMMA films of different thicknesses h ($\tau_{PMMA} = 30$ ps, $\delta = 2.0 \times 10^{-3}$ cm^2/s and $f = 0.35$) deposited on substrates of Au ($\tau = 1$ ns, $\delta = 1.28$ cm^2/s and $f = 0.02$) and SiO_2 ($\tau = 40$ ps, $\delta = 4.1 \times 10^{-3}$ and $f = 0.35$). (d–h) Momentum maps in the ρ-z plane (similar input parameters as above). The isomomentum lines at $p_z = 0.40$ define the crater boundaries. (d, e) Freestanding PMMA layers of 40 nm (d) and 5 nm (e); note the momentum inversion at $z = h/2$, limiting crater depth to $h/2$ in ultrathin films. (f, g) 5 nm thick PMMA on Au calculated with $f = 0.02$ (f) and $f = 0.35$ (g). (h, i) 5 nm PMMA on SiO_2 calculated with $\delta_{SiO_2} = 4.1 \times 10^{-3}$ cm^2/s (h) and $\delta_{SiO_2} = 0.83 \times 10^{-3}$ cm^2/s. The dashed lines depict the substrate/polymer interface.

enhancement in films with thicknesses between 15 and 30 nm due to contributions of excitation from the substrate, but decreases again in thinner films due to reductions of impulses from the polymer layer itself.

In several aspects qualitative trends predicted by the analytical model are observed in the experiments. This includes the enhancement of the rim volume and crater depth in the films deposited on silica, as compared to Au, and the consequent shift toward lower thicknesses of the critical depth h_c. However, the measured enhancement of the impact feature sizes in films deposited on SiO_2 is much weaker than expected. In particular, the insensitivity of the crater diameter to the type of underlying substrate, evidenced experimentally even in very thin films, is in striking disagreement with the model calculations. Even if the contribution of the SiO_2 substrate is made weaker by using smaller values of δ (as in Fig. 4i) or τ and dE/dx_{eff} (Figs. S2 and S3), the increase in crater diameters with decreasing h persists. Moreover, the experimental crater sizes are very similar for the Si and SiO_2 substrates. Judging from bulk transport properties of crystalline Si (much larger values of δ and τ than PMMA or silica) and the much shorter ion track lifetime compared to insulators [47] (i.e, f is small for Si), the influence of Si according to the model should not be much different from Au. The presence of the native oxide layer on Si surfaces could explain the similarities between both substrates, but based on the calculations, only silica films thicker than ~10 nm would be equivalent to bulk silica (see Fig. S4).

4. Conclusions

In summary, we provide direct experimental evidence that fast-ion-induced crater and rim formation in ultrathin polymer films are directly affected by the underlying substrate to a degree that depends on the material's electrical and thermal properties. Calculations from a numerical model based on linear additivity and diffusive transport of the excitation energy describe the effects partially. Discrepancies between the experiments and model predictions suggest that the actual energy exchange at the substrate/polymer interface is low. Other factors, beyond pure diffusive transport and related to interfacial processes, including adhesion and roughness may play a role. For example, strain waves generated by the ion impact (which seems to be important for cratering in soft materials [4,8]) would be strongly reflected at the polymer/substrate interface because of the large acoustic impedance mismatch between the media. This mismatch would also decouple momentum transfer between layers. Our results stress the importance of careful consideration of nanomaterials' surroundings for a precise determination of their response to ion radiation.

Declaration of competing interest

The authors declare that they have no known competing financial interests or personal relationships that could have appeared to influence the work reported in this paper.

Acknowledgements

This work was supported by Brazilian foundations National Council for Scientific and Technological Development (CNPq, Grant Nos. 117750/2017-4 and 404301/2016-9) and Coordination for the Improvement of Higher Education Personnel (CAPES, Grant Nos. 88887.176042/2018-00 and 88882.314866/2019-01 and Finance Code 001) as well as the National Institute of Surface Engineering (INES) and PRONEX-FAPERGS (Grant No. 16/2551-0000479-0). The sample irradiation is part of the experiment UMAT, which was performed at the beam line X0 at the GSI Helmhotzzentrum für Schwerionenforschung, Darmstadt (Germany) in the frame of FAIR Phase-0.

Appendix A. Supplementary data

Supplementary data to this article can be found online at https://doi.org/10.1016/j.cap.2021.10.004.

References

[1] R. Fleischer, P. Price, R. Walker, Nuclear Tracks in Solids: Principles and Applications, University of California Press, 1975.
[2] R. Spohr, Ion Tracks and Microtechnology: Principles and Applications, Springer Vieweg Verlag, 1990.
[3] S. Klaumünzer, M.-D. Hou, G. Schumacher, Coulomb explosions in a metallic-glass due to the passage of fast heavy-ions, Phys. Rev. Lett. 57 (7) (1986) 850–853, https://doi.org/10.1103/PhysRevLett.57.850.
[4] R. Johnson, B. Sundqvist, A. Hedin, D. Fenyo, Sputtering by fast ions based on a sum of impulses, Phys. Rev. B 40 (1) (1989) 49–53, https://doi.org/10.1103/PhysRevB.40.49.
[5] M. Toulemonde, C. Dufour, E. Paumier, Transient thermal-process after a high-energy heavy-ion irradiation of amorphous metals and semiconductors, Phys. Rev. B 46 (22) (1992) 14362–14369, https://doi.org/10.1103/PhysRevB.46.14362.
[6] A. Meftah, F. Brisard, J.M. Costantini, E. Dooryhee, M. Hage-Ali, M. Hervieu, J. P. Stoquert, F. Studer, M. Toulemonde, Track formation in sio$_2$ quartz and the thermal-spike mechanism, Phys. Rev. B 49 (18) (1994) 12457–12463, https://doi.org/10.1103/PhysRevB.49.12457.
[7] P. Kluth, C.S. Schnohr, O.H. Pakarinen, F. Djurabekova, D.J. Sprouster, R. Giulian, M.C. Ridgway, A.P. Byrne, C. Trautmann, D.J. Cookson, K. Nordlund, M. Toulemonde, Fine structure in swift heavy ion tracks in amorphous SiO_2, Phys. Rev. Lett. 101 (17) (2008) 175503, https://doi.org/10.1103/PhysRevLett.101.175503.
[8] J. Eriksson, J. Rottler, C.T. Reimann, Fast-ion-induced surface tracks in bioorganic films, Int. J. Mass Spectrom. 175 (3) (1998) 293–308, https://doi.org/10.1016/s0168-1176(98)00123-2.
[9] E. Akcoltekin, T. Peters, R. Meyer, A. Duvenbeck, M. Klusmann, I. Monnet, H. Lebius, M. Schleberger, Creation of multiple nanodots by single ions, Nat. Nanotechnol. 2 (5) (2007) 290–294, https://doi.org/10.1038/nnano.2007.109.
[10] L.I. Gutierres, N.W. Lima, R. Thomaz, R.M. Papaléo, E.M. Bringa, Simulations of cratering and sputtering from an ion track in crystalline and amorphous Lennard Jones thin films, Comput. Mater. Sci. 129 (2017) 98–106, https://doi.org/10.1016/j.commatsci.2016.12.001.
[11] L. Farenzena, R. Livi, M. de Araujo, G. Bermudez, R. Papaleo, Cratering and plastic deformation in polystyrene induced by mev heavy ions: dependence on the molecular weight, Phys. Rev. B 63 (10) (2001), https://doi.org/10.1103/PhysRevB.63.104108.
[12] I. Alencar, M.R. Silva, R. Leal, P.L. Grande, R.M. Papaléo, Impact features induced by single fast ions of different charge-state on muscovite mica, Atoms 9 (2021) 17, https://doi.org/10.3390/atoms9010017.
[13] R.M. Papaleo, M.R. Silva, R. Leal, P.L. Grande, M. Roth, B. Schattat, G. Schiwietz, Direct evidence for projectile charge-state dependent crater formation due to fast ions, Phys. Rev. Lett. 101 (16) (2008) 167601, https://doi.org/10.1103/PhysRevLett.101.167601.
[14] R. Papaléo, L. Farenzena, M. de Araujo, R. Livi, M. Alurralde, G. Bermudez, Cratering in PMMA induced by gold ions: dependence on the projectile velocity, Nucl. Instrum. Methods Phys. Res. Sect. B Beam Interact. Mater. Atoms 148 (1–4) (1999) 126–131, https://doi.org/10.1016/S0168-583X(98)00877-5.
[15] R. Papaleo, R. Leal, C. Trautmann, E. Bringa, Cratering by MeV-GeV ions as a function of angle of incidence, Nucl. Instrum. Methods Phys. Res. Sect. B Beam Interact. Mater. Atoms 206 (2003) 7–12, https://doi.org/10.1016/S0168-583X(03)00683-9.
[16] R.M. Papaléo, Surface tracks and cratering in polymers, in: Transport Processes in Ion-Irradiated Polymers, Springer, 2004, pp. 207–250.
[17] R. Neumann, Scanning probe microscopy of ion-irradiated materials, Nucl. Instrum. Methods Phys. Res. Sect. B Beam Interact. Mater. Atoms 151 (1–4) (1999) 42–55, https://doi.org/10.1016/s0168-583x(99)00136-6. URL <Go to ISI>://WOS:000080604100006.
[18] M. Kobylko, P.-E. Coulon, A. Slablab, A. Fafin, J. Cardin, C. Dufour, A. Losquin, M. Kociak, I. Monnet, D. Mailly, X. Lafosse, C. Ulysse, E. Garcia-Caurel, G. Rizza, Localized plasmonic resonances of prolate nanoparticles in a symmetric environment: experimental verification of the accuracy of numerical and analytical models, Phys. Rev. Appl. 9 (6) (2018), 064038, https://doi.org/10.1103/PhysRevApplied.9.064038.
[19] K. Amemiya, H. Koshikawa, M. Imbe, T. Yamaki, H. Shitomi, Perfect blackbody sheets from nano-precision microtextured elastomers for light and thermal radiation management, J. Mater. Chem. C 7 (18) (2019) 5418–5425, https://doi.org/10.1039/c8tc06593d.
[20] G. Laucirica, M.E. Toimil-Molares, C. Trautmann, W. Marmisoll, O. Azzaroni, Polyaniline for improved blue energy harvesting: highly rectifying nanofluidic diodes operating in hypersaline conditions via one-step functionalization, ACS Appl. Mater. Interfaces 12 (25) (2020) 28148–28157, https://doi.org/10.1021/acsami.0c05102.
[21] G. Battistoni, I. Mattei, S. Muraro, Nuclear physics and particle therapy, Adv. Phys-X 1 (4) (2016) 661–686, https://doi.org/10.1080/23746149.2016.1237310.
[22] E. Balanzat, S. Bouffard, A. Le Moël, N. Betz, Physico-chemical modifications induced in polymers by swift heavy ions, Nucl. Instrum. Methods Phys. Res. Sect. B Beam Interact. Mater. Atoms 91 (1) (1994) 140–145, https://doi.org/10.1016/0168-583X(94)96204-9.
[23] E.H. Lee, Ion-beam modification of polymeric materials – fundamental principles and applications, Nucl. Instrum. Methods Phys. Res. Sect. B Beam Interact. Mater. Atoms 151 (1) (1999) 29–41, https://doi.org/10.1016/S0168-583X(99)00129-9.

[24] J.O. Choi, J.A. Moore, J.C. Corelli, J.P. Silverman, H. Bakhru, Degradation of poly(methylmethacrylate) by deep ultraviolet, x- ray, electron beam, and proton beam irradiations, J. Vac. Sci. Technol. B: Microelectron. Nanometer Struct. 6 (1988) 2286, https://doi.org/10.1116/1.584071.
[25] E.H. Lee, G.R. Rao, L.K. Mansur, LET effect on cross- linking and scission mechanisms of pmma during irradiation, Radiat. Phys. Chem. 55 (3) (1999) 293–305.
[26] B. Pignataro, M. Fragala, O. Puglisi, AFM and XPS study of ion bombarded poly (methyl methacrylate), Nucl. Instrum. Methods Phys. Res. Sect. B Beam Interact. Mater. Atoms 131 (1–4) (1997) 141–148, https://doi.org/10.1016/S0168-583X(97)00297-8.
[27] F. Schrempel, W. Witthuhn, Deep light ion lithography in PMMA - a parameter study, Nucl. Instrum. Methods Phys. Res. Sect. B Beam Interact. Mater. Atoms 132 (3) (1997) 430–438.
[28] M. Komuro, N. Atoda, H. Kawakatsu, Ion-beam exposure of resist materials, J. Electrochem. Soc. 126 (3) (1979) 483–490, https://doi.org/10.1149/1.2129067.
[29] T.M. Hall, A. Wagner, L.F. Thompson, Ion beam exposure characteristics of resists: experimental results, J. Appl. Phys. 53 (6) (1982) 3997–4010, https://doi.org/10.1063/1.331261.
[30] S. Gorelick, V.A. Guzenko, J. Vila-Comamala, C. David, Direct e-beam writing of dense and high aspect ratio nanostructures in thick layers of pmma for electroplating, Nanotechnology 21 (29) (2010) 8, https://doi.org/10.1088/0957-4484/21/29/295303. URL <Go to ISI>://WOS:000279459300006.
[31] Y. Vladimirsky, O. Vladimirsky, K.J. Morris, J.M. Klopf, G.M. Calderon, V. Saile, PMMA as an x-ray resist for micro-machining application: latent image formation and thickness losses, Microelectron. Eng. 30 (1–4) (1996) 543–546, https://doi.org/10.1016/0167-9317(95)00305-3.
[32] N. Puttaraksa, R. Norarat, M. Laitinen, T. Sajavaara, S. Singkarat, H.J. Whitlow, Lithography exposure characteristics of poly(methyl methacrylate) (PMMA) for carbon, helium and hydrogen ions, Nucl. Instrum. Methods Phys. Res., Sect. B 272 (2012) 162–164, https://doi.org/10.1016/j.nimb.2011.01.056.
[33] J.A. van Kan, P. Malar, Y.H. Wang, Resist materials for proton beam writing: a review, Appl. Surf. Sci. 310 (2014) 100–111, https://doi.org/10.1016/j.apsusc.2014.04.147.
[34] U. Linz, Ion Beam Therapy: Fundamentals, Technology, Clinical Applications, Springer Berlin Heidelberg, 2011.
[35] D. Schardt, T. Elsaesser, D. Schulz-Ertner, Heavy-ion tumor therapy: physical and radiobiological benefits, Rev. Mod. Phys. 82 (1) (2010) 383–425, https://doi.org/10.1103/RevModPhys.82.383.
[36] J.S. Loeffler, M. Durante, Charged particle therapy-optimization, challenges and future directions, Nat. Rev. Clin. Oncol. 10 (7) (2013) 411–424, https://doi.org/10.1038/nrclinonc.2013.79.
[37] C. Trautmann, Micro- and nanoengineering with ion tracks, in: Ion Beams in Nanoscience and Technology, Springer, Heidelberg, 2010, pp. 369–387.
[38] A.V. Krasheninnikov, K. Nordlund, Ion and electron irradiation-induced effects in nanostructured materials, J. Appl. Phys. 107 (7) (2010), 071301, https://doi.org/10.1063/1.3318261.
[39] E.M. Bringa, J.D. Monk, A. Caro, A. Misra, L. Zepeda-Ruiz, M. Duchaineau, F. Abraham, M. Nastasi, S.T. Picraux, Y.Q. Wang, D. Farkas, Are nanoporous materials radiation resistant? Nano Lett. 12 (7) (2012) 3351–3355, https://doi.org/10.1021/nl201383u.
[40] G. Greaves, J.A. Hinks, P. Busby, N.J. Mellors, A. Ilinov, A. Kuronen, K. Nordlund, S.E. Donnelly, Enhanced sputtering yields from single-ion impacts on gold nanorods, Phys. Rev. Lett. 111 (6) (2013), 065504, https://doi.org/10.1103/PhysRevLett.111.065504.
[41] C. Sun, S. Zheng, C.C. Wei, Y. Wu, L. Shao, Y. Yang, K.T. Hartwig, S.A. Maloy, S. J. Zinkle, T.R. Allen, H. Wang, X. Zhang, Superior radiation-resistant nanoengineered austenitic 304L stainless steel for applications in extreme radiation environments, Sci. Rep. 5 (2015) 7801.
[42] A. Johannes, S. Noack, W. Wesch, M. Glaser, A. Lugstein, C. Ronning, Anomalous plastic deformation and sputtering of ion irradiated silicon nanowires, Nano Lett. 15 (6) (2015) 3800–3807, https://doi.org/10.1021/acs.nanolett.5b00431.
[43] P.I. Gaiduk, C. Trautmann, Tracks in epitaxial $Si_{1-x}Ge_x$ alloy layers: effect of layer thickness, Nucl. Instrum. Methods Phys. Res. Sect. B Beam Interact. Mater. Atoms 256 (1) (2007) 224–228, https://doi.org/10.1016/j.nimb.2006.12.007.
[44] R.K. Pandey, M. Kumar, S.A. Khan, T. Kumar, A. Tripathi, D.K. Avasthi, A. C. Pandey, Study of electronic sputtering of CaF_2 thin films, Appl. Surf. Sci. 289 (2014) 77–80, https://doi.org/10.1016/j.apsusc.2013.10.102.
[45] R. Thomaz, P. Louette, G. Hoff, S. Müller, J.J. Pireaux, C. Trautmann, R. M. Papaléo, Bond-breaking efficiency of high-energy ions in ultrathin polymer films, Phys. Rev. Lett. 121 (6) (2018), 066101, https://doi.org/10.1103/PhysRevLett.121.066101.
[46] R.M. Papaléo, R. Thomaz, L.I. Gutierres, V.M. de Menezes, D. Severin, C. Trautmann, D. Tramontina, E.M. Bringa, P.L. Grande, Confinement effects of ion tracks in ultrathin polymer films, Phys. Rev. Lett. 114 (11) (2015) 118302, https://doi.org/10.1103/PhysRevLett.114.118302.
[47] G. Schiwietz, K. Czerski, R. Hellhammer, A. Roth, F. Staufenbiel, R.C. Fadanelli, P. L. Grande, Search for short-time phase effects in the electronic damage evolution: a case study with silicon, Nucl. Instrum. Methods Phys. Res. Sect. B Beam Interact. Mater. Atoms 266 (8) (2008) 1287–1293, https://doi.org/10.1016/j.nimb.2007.11.048.
[48] Y. Feng, Z. Zhou, Y. Zhou, G. Zhao, Cross sections for 165° backscattering from carbon, Nucl. Instrum. Methods Phys. Res. Sect. B Beam Interact. Mater. Atoms 86 (1994) 225–230, https://doi.org/10.1016/0168-583X(94)95282-5.
[49] M. Mayer, SIMNRA User's Guide, Report IPP 9/113, Max-Planck-Institut für Plasmaphysik, Garching, Germany, 1997.
[50] K.I. Chan, Experimental Investigation of Size Effect on Thermal Conductivity for Ultra-thin Amorphous Poly(methyl Methacrylate) (PMMA) Films, Master's thesis, Texas A&M University, Texas, 2007.
[51] E.M. Bringa, R.E. Johnson, R.M. Papaléo, Crater formation by single ions in the electronic stopping regime: comparison of molecular dynamics simulations with experiments on organic films, Phys. Rev. B 65 (9) (2002), 094113, https://doi.org/10.1103/PhysRevB.65.094113.
[52] H.D. Mieskes, W. Assmann, F. Grüner, H. Kucal, Z.G. Wang, M. Toulemonde, Electronic and nuclear thermal spike effects in sputtering of metals with energetic heavy ions, Phys. Rev. B 67 (2003) 155414, https://doi.org/10.1103/PhysRevB.67.155414.
[53] M. Toulemonde, Private Communication.
[56] C.J. Morath, H.J. Maris, Phonon attenuation in amorphous solids studied by picosecond ultrasonics, Phys. Rev. B 54 (1) (1996) 203–213, https://doi.org/10.1103/PhysRevB.54.203.
[60] N.W. Lima, L.I. Gutierres, R.I. Gonzalez, S. Müller, R.S. Thomaz, E.M. Bringa, R. M. Papaléo, Molecular dynamics simulation of polymerlike thin films irradiated by fast ions: a comparison between FENE and Lennard-Jones potentials, Phys. Rev. B 94 (2016) 195417, https://doi.org/10.1103/PhysRevB.94.195417.